THE JOURNAL OF BIOLOGICAL CHEMISTRY VOL. 287, NO. 50, pp. 42180–41294, December 7, 2012

Isocitrate Dehydrogenase (IDH) Mutations Promote a Reversible ZEB1/MicroRNA (miR)-200-dependent Epithelial-Mesenchymal Transition (EMT)*[S]

Received for publication, September 9, 2012, and in revised form, October 3, 2012 Published, JBC Papers in Press, October 4, 2012, DOI 10.1074/jbc.M112.417832

Alexandra R. Grassian[‡1], Fallon Lin[‡], Rosemary Barrett[‡], Yue Liu[‡], Wei Jiang[‡], Manav Korpal[‡1], Holly Astley[§], Daniel Gitterman[§], Thomas Henley[§], Rob Howes[§], Julian Levell[‡], Joshua M. Korn[‡], and Raymond Pagliarini[‡2]

From the [‡]Novartis Institutes for Biomedical Research, Cambridge, Massachusetts 02139 and [§]Horizon Discovery Ltd., 7100 Cambridge Research Park, Waterbeach, Cambridge, CB25 9TL, United Kingdom

Background: Isocitrate dehydrogenase (IDH) mutations occur in diverse tumor types, leading to production of the oncometabolite 2-hydroxyglutarate (2-HG).
Results: High 2-HG levels lead to a reversible epithelial-mesenchymal transition (EMT) phenotype, which is dependent on ZEB1/miR-200.
Conclusion: Mutant IDH reversibly disrupts normal epithelial morphology through EMT induction, a possible tumorigenic mechanism.
Significance: This is the first report of a reversible mutant IDH-dependent signaling phenotype.

Mutations in the genes encoding isocitrate dehydrogenase 1 and 2 (IDH1/2) occur in a variety of tumor types, resulting in production of the proposed oncometabolite, 2-hydroxyglutarate (2-HG). How mutant IDH and 2-HG alter signaling pathways to promote cancer, however, remains unclear. Additionally, there exist relatively few cell lines with IDH mutations. To examine the effect of endogenous IDH mutations and 2-HG, we created a panel of isogenic epithelial cell lines with either wild-type IDH1/2 or clinically relevant IDH1/2 mutations. Differences were noted in the ability of IDH mutations to cause robust 2-HG accumulation. IDH1/2 mutants that produce high levels of 2-HG cause an epithelial-mesenchymal transition (EMT)-like phenotype, characterized by changes in EMT-related gene expression and cellular morphology. 2-HG is sufficient to recapitulate aspects of this phenotype in the absence of an IDH mutation. In the cells types examined, mutant IDH-induced EMT is dependent on up-regulation of the transcription factor ZEB1 and down-regulation of the miR-200 family of microRNAs. Furthermore, sustained knockdown of IDH1 in IDH1 R132H mutant cells is sufficient to reverse many characteristics of EMT, demonstrating that continued expression of mutant IDH is required to maintain this phenotype. These results suggest mutant IDH proteins can reversibly deregulate discrete signaling pathways that contribute to tumorigenesis.

Recurrent somatic mutations in the NADPH-dependent isocitrate dehydrogenase genes IDH1 and IDH2 have recently been identified in a wide variety of cancer types, including subsets of acute myeloid leukemia (AML),[3] gliomas, and secondary glioblastoma multiforme, cholangiocarcinoma, chondrosarcoma, supratentorial primordial neuroectodermal tumors, and peripheral T-cell lymphoma (1–11). Albeit more rarely, IDH1/2 mutations are also observed in melanoma (12) and epithelial tumors of the prostate, lung, and colon (13–17). These findings implicate IDH1 and -2 mutations as a key emerging driver of tumorigenesis in a wide variety of tumor lineages.

The IDH1/2 mutations recurrently identified in cancers are almost always heterozygous point mutations that occur in one of only a few residues in the catalytic pocket (*IDH1*, Arg-132; *IDH2*, Arg-140 and Arg-172), a genetic "signature" for activating oncogenic mutations (18, 19). Although IDH mutants are no longer capable of efficiently carrying out their normal "forward" reactions (isocitrate to α-ketoglutarate (αKG)), IDH mutations confer a novel gain-of-function and can efficiently catalyze a modified "reverse" reaction, converting αKG to 2-hydroxyglutarate (2-HG) (6, 20). 2-HG is not normally present at high levels but is found at very high levels in the tumors of patients with IDH1/2 mutations (6, 20). Interestingly, 2-HG also accumulates in patients with inactivating mutations in the 2-hydroxyglutarate dehydrogenase genes (*D2HGDH* and *L2HGDH*) and is associated with the development of brain tumors (21, 22), suggesting that 2-HG may directly contribute to cancer and thus may be an "oncometabolite."

The similarity of 2-HG to αKG has led to the hypothesis that the oncogenic function of 2-HG may be through alteration of αKG-dependent enzyme function (19). αKG-dependent enzymes control a wide variety of cellular processes, including

* A. R. G., F. L., R. B., Y. L., M. K., J. L., J. M. K., and R. P. are all employees of Novartis Institutes for BioMedical Research. H. A., D. G., T. H., and R. H. are all employees of Horizon Discovery.

[S] This article contains supplemental Figs. S1–S4 and Tables S1 and S2.

The nucleotide sequence(s) reported in this paper has been submitted to the GenBank™/EBI Data Bank with accession number(s) GSE4180.

[1] Recipients of presidential postdoctoral fellowships from Novartis Institutes for Biomedical Research.

[2] To whom correspondence should be addressed: Novartis Institutes for Biomedical Research, 250 Massachusetts Ave., Cambridge, MA 02139. Tel.: 617-871-4307; E-mail: raymond.pagliarini@novartis.com.

[3] The abbreviations used are: AML, acute myeloid leukemia; IDH, isocitrate dehydrogenase; 2-HG, 2-hydroxyglutarate; αKG, α-ketoglutarate; EMT, epithelial-mesenchymal transition; NTC, nontargeting control; qRT-PCR, quantitative real time PCR; miR-200, microRNA200; miRNA, microRNA.

deregulation of the hypoxic response, modification of the collagen matrix, and the turnover of DNA and histone methylation, leading to potentially global changes in gene expression and cellular biology (23). Thus far, mutant IDH1/2 and/or 2-HG have been reported to correlate with and/or affect all of these processes (24–33).

At odds with the potential of 2-HG to modify multiple epigenetic and cellular processes is the observation that 2-HG accumulation has strikingly specific effects on altering cellular differentiation, as observed in neural, hematopoietic, and adipogenic cell types (26–28, 30, 32, 34), suggesting IDH1/2 mutations may deregulate discrete signaling pathways that depend on the cell background or lineage. Because of the general lack of IDH1/2 mutant cell lines (35), most studies have relied on mutant IDH overexpression; it is unclear, however, if the biology observed in such models accurately recapitulates the role of endogenously expressed mutant IDH in the initiation and progression of clinically observed cancers.

To address this question, we generated a panel of HCT116 colorectal cancer cells and MCF-10A mammary epithelial cells with endogenously expressed, heterozygous, and clinically relevant *IDH1/2* mutations. Our characterization of these cell lines suggests differences in the ability of these IDH1/2 mutations to produce 2-HG in cells, an observation that allowed for the separation of the effects of 2-HG from the IDH mutation. From this, we observe that 2-HG accumulation, rather than IDH1/2 mutational status alone, has more dramatic effects on altering cellular signaling. Specifically, we observe a direct correlation between intracellular 2-HG levels and an epithelial-mesenchymal transition (EMT)-like phenotype, characterized by changes in both morphology and expression of EMT markers. Addition of exogenous 2-HG is sufficient on its own to induce similar EMT-like alterations in IDH1/2 wild-type cells. Mutant IDH1/2 and 2-HG up-regulate ZEB1 and down-regulate miR-200, two key drivers of the EMT process. We demonstrate that this deregulation of ZEB1 and miR-200 is necessary to drive EMT-like phenotypes downstream of mutant IDH1/2. Finally, sustained knockdown of IDH1 in an IDH1 R132H mutant clone is able to reverse many aspects of the EMT-like phenotype, demonstrating that mutant IDH phenotypes are reversible, albeit with surprisingly slow kinetics. Thus, our data demonstrate that mutant IDH1/2 can regulate specific signaling pathways that remain dependent on continued mutant IDH expression and provide insight into core pathways that may be deregulated in epithelial tumors that bear the IDH1/2 mutation.

EXPERIMENTAL PROCEDURES

Generation of Endogenously Heterozygous IDH1/2 Mutant Cells—HCT116 or MCF-10A cells with endogenously heterozygous mutations in *IDH1/2* were generated via recombinant adeno-associated virus technology, as described previously (36). These cell lines were sequence-verified at both the genomic and RNA levels. Note that one of the clones (HCT116 R132C/+ 16F8) contains the IDH1 R132C mutation at the DNA level but not at the RNA level and thus is utilized as a nonexpressing control. Detailed information regarding the targeting and production of these cells lines is available upon request.

Cell Culture—HCT116 cells were cultured in McCoy's 5A modified medium with 10% fetal bovine serum. 2-HG treatments were done at 10 mM and replenished every 48 h. MCF-10A cells were cultured as described previously (37). Exogenous 2-HG treatments were done at 10 mM, and fresh 2-HG was added every 2 days. For all light microscopy images of cells, images were taken on a Nikon Eclipse TE2000-U with phase contrast microscopy using a Nikon Digital Camera DXM 1200. Representative images are shown, and scale bars represent 50 μm.

Immunofluorescence—Cells were cultured in 8-well chamber slides (BD Biosciences) and fixed in 4% paraformaldehyde for 10 min, rinsed in PBS, permeabilized in 0.2% Triton X-100 in PBS for 5 min, and then rinsed in PBS. Primary antibodies (ZO-1 (Invitrogen, 61-7300) and β-catenin (BD Biosciences, 610154)) were incubated in PBS for 1 h, followed by PBS rinsing, and then fluorophore-conjugated secondary antibodies were incubated in PBS. After PBS washing, cells were then mounted in Prolong Gold Antifade (Invitrogen). Images were taken on a Zeiss Axiovert 200 M. Representative images are shown, and scale bars represent 50 μm.

Synthesis of Sodium (R)-2-Hydroxypentanedioate ((R)-2-Hydroxyglutaric Acid Disodium Salt)—For step 1, a solution of sodium nitrite (16.56 g, 240 mmol) in water (50 ml) was added dropwise at 0–5 °C to a stirred mixture of D-glutamic acid (29.44 g, 200 mmol), water (80 ml), and concentrated hydrochloric acid (52.6 ml, 520 mmol). After complete addition, the reaction mixture was allowed to warm slowly to room temperature overnight. The volatile components were evaporated *in vacuo* at 50–60 °C. The residue was triturated with hot EtOAc (4× 150 ml). Each time the hot EtOAc was decanted from the undissolved solids. The combined EtOAc solutions were cooled, dried (Na_2SO_4), concentrated to dryness, and placed under high vacuum for 72h to give (*R*)-5-oxotetrahydrofuran-2-carboxylic acid (11.77 g, 45%) as a white waxy solid. ^{1}H NMR in CDCl3 suggests ~15 mol % of the ring open 2-HG (relative integral of peaks at δ 4.43 ppm for 2-HG *versus* δ 4.95 ppm for lactone). This material was used as-is in the following step: (*R*)-5-oxotetrahydrofuran-2-carboxylic acid ^{1}H NMR (CDCl3) δ 10.88 (H, br s), 4.98–4.93 (H, m), 2.65–2.49 (3H, m), 2.40–2.30 (H, m); diagnostic peak for 2-HG, δ 4.43 (H, dd, J 8,6 Hz).

For step 2, (*R*)-5-oxotetrahydrofuran-2-carboxylic acid (11.77 g, 90 mmol) was dissolved in MeOH (50 ml), treated with NaOH (8 g, 200 mmol) in water (100 ml), and stirred for 2 h at room temperature (initial exotherm and slight yellow coloration observed). The reaction mixture was kept at pH 14. The reaction mixture was sampled and concentrated to dryness, and ^{1}H NMR of sample showed the reaction was complete. The reaction mixture was concentrated to the point where the solid started to precipitate from the solution, and MeCN (30 ml) was then added followed by sufficient methanol to give one phase, followed by additional methanol (50 ml). The white precipitate was filtered off, suspended in 5% water/MeOH (100 ml), filtered, and washed with 50:50 methanol/MeCN followed by neat MeCN. The solid was dried under high vacuum to give sodium (*R*)-2-hydroxypentanedioate (13.06 g, 75%) (also

known as (*R*)-2-hydroxyglutaric acid disodium salt) as a white crystalline powder. For ^{1}H NMR (D_2O), δ 3.93 (H, dd, *J* 8,6 Hz), 2.25–2.10 (2H, m), 1.96–1.86 (H, m), and 1.80–1.69 (H, m).

Immunoblotting—Cells were lysed in RIPA buffer (Boston Bioproducts) containing Halt Protease and Phosphatase Inhibitor Mixture (Thermo Scientific). Lysates were spun at 16,000 × *g* at 4 °C for 30 min and normalized for protein concentration. Lysates were then subjected to SDS-PAGE, and transfer/blotting was performed as described previously (38). Blots were imaged either by chemiluminescence or by fluorescent imaging using the Odyssey infrared imaging system (LI-COR Biosciences; Millennium Science, Surrey Hills, Australia). The following antibodies were used: IDH1 R132H (Dianova, H09), IDH2 (Abcam, ab55271), ZEB1 (Cell Signaling Technology, 3396), E-cadherin (Cell Signaling Technology, 3195), fibronectin (Abcam, ab2413), GAPDH (Millipore, MAB374), and β-tubulin (Abcam, ab6046). Total IDH1 antibody is a rabbit polyclonal antibody produced through immunization with recombinant IDH1 protein. Detailed information on this antibody is available upon request.

Microarray—Total RNA was isolated from cells using the Qiagen RNeasy kit. RNA integrity and purity were assessed with the RNA 6000 Nano LabChip system on a Bioanalyzer 2100 (Agilent Technologies). Generation of labeled cDNA and hybridization to Affymetrix GeneChip Human Genome U133 Plus 2.0 Array (Affymetrix Inc.) were performed using standard protocols as described previously (39).

Expression Analysis—Probe sets from the Affymetrix gene expression datasets were normalized using MAS5 with a trimmed mean target of 150 and $\log_2$-transformed. Probe sets were then filtered for inclusion only if their maximum value over different samples was at least 5. Ordinary least squares were performed using a 0–1 indicator variable as the sole covariate; once the indicator represented clones with expressed mutant IDH and once the indicator represented clones with high 2-HG levels. This regression was used to generate nominal *p* values and regression coefficients (*i.e.* fold-changes). Individual probe sets were considered significantly differentially expressed if their fold-change was ≥2, with a nominal *p* value of ≤0.01.

Pathway Enrichment Scores—For the candidate signatures (40–42), a two-tailed Fisher's exact test was used to determine whether probe sets representing genes in those signatures were under- or over-represented in the set of probe sets that were up- or down-regulated at least 1.5-fold compared with expressed but nondifferentially expressed probe sets with a nominal *p* value of 0.05 or less. For an unbiased approach, pathways derived from GO terms and transcription factor networks were analyzed for over-representation via a one-tailed interpolated Fisher's exact test, using genes that varied 1.5-fold or more with a nominal *p* value of 0.05 or less compared with all genes represented on the array; Benjamini-Hochberg correction was then applied to these *p* values (39).

Analysis of mRNA and miRNA Levels—Total RNA was isolated from cells using the RNeasy kit (Qiagen). cDNA was synthesized from 2 μg of RNA using the iScript cDNA synthesis kit (Bio-Rad). Real time PCR was performed using an ABI PRISM 7900HT fast real time PCR system with gene-specific primers and FastStart Universal Probe Master (Rox) (Roche Applied Science). The following gene-specific primers (Invitrogen) were used: E-cadherin (Hs01023894_m1), fibronectin (Hs00365052_m1), IDH1 (Hs01855675_s1), vimentin (Hs00185584_m1), ZEB1 (Hs00232783_m1), and ZEB2 (Hs00207691_m1). Quantification of relative mRNA expression levels was determined and normalized to β_2-microglobulin (Hs00984230_m1) expression.

For miRNA analysis, mature miRNA were reverse-transcribed from 10 ng of RNA using the TaqMan microRNA reverse transcription kit (Invitrogen). Real time PCR was performed using an ABI PRISM 7900HT fast real time PCR system with TaqMan microRNA assays for miR-200b (Assay ID 002251) or miR-200c (Assay ID 002300) and Taqman Universal Master Mix II (Invitrogen). All data were normalized to small nucleolar RNA, C/D box 44 (RNU44 - Assay ID 001094) expression.

miRNA Mimetics—The following miRIDIAN microRNA mimics (Thermo Fisher Scientific) were used: miRIDIAN microRNA mimic negative control 1 (CN-001000-01), miRIDIAN mimic hsa-miR-200b (C-300582-07), and miRIDIAN mimic hsa-miR-200c (C-300646-05). Cells were transfected with DharmaFECT DUO transfection reagent as per the manufacturer's instructions. mRNA, protein, and morphology changes were assessed 72 h after transfection.

RNA Interference—The following small interfering RNA (siRNA) reagents (Dharmacon, Lafayette, CO) were used: nontargeting control (D-001810-01); ZEB1, J-006564-11 ("A"), J-006564-12 ("B"), and J-006564-13 ("C"). For each transfection, 30 pmol of siRNA were transfected into cells using RNAiMax (Invitrogen) with 2.5 ml of growth media, according to the manufacturer's protocol. Knockdown efficiency was examined after 72 h by immunoblotting and qRT-PCR.

IDH1 shRNAs were generated in pLKO-based lentiviral vectors containing a tetracycline-inducible promoter as described previously (43). The targeting sequences for the IDH1 shRNAs were as follows: IDH1 shRNA A, GGAATCCGGAATAAATACTAC, and IDH1 shRNA B, GCCTGGCCTGAATATTATACT. The HCT116 IDH1 R132H/+ 2H1 clone was transduced with these shRNAs or a nontargeting control (43). After viral transduction, 0.6 μg/ml puromycin was added to select for polyclonal pools of cells with stable integration of the shRNA constructs. For all experiments, cells were grown in the presence of 100 ng/ml doxycycline where noted for the indicated number of days to induce shRNA expression.

cDNA Expression—cDNA constructs encoding the IDH2 mutants R140Q and R172K were subcloned into the pLKO-TREX-HA vector (44). Stably transduced pools were selected in 0.6 μg/ml puromycin. Cells were cultured as above.

2-HG Quantification—Cells were trypsinized, and pellets of 1 million cells were collected and stored at −80 °C until extracted. Extractions were performed in 80% methanol kept at −80 °C, and samples were then sonicated in an ice-water bath for 10 min. Samples were then vortexed until pellets were resuspended, placed on dry ice for a minimum of 30 min, and centrifuged at 14,000 rpm for 10 min. The supernatant was used for 2-HG quantification by LC-MS/MS analysis.

An AB Sciex 4000 triple quadrupole mass spectrometer (Foster City, CA) equipped with an Agilent 1200 series HPLC sys-

tem (Santa Clara CA) and a CTC auto sampler (Carrboro, NC) was used for the analysis. The mass spectrometer was operated in the ESI negative ionization multiple reaction monitoring (transition 147→129) mode with a spray voltage of −4500 V. Ion source gas 1, ion source gas 2, and curtain gas were set at 50, 35, and 25 p.s.i., respectively, and the source temperature was maintained at 550 °C. Separations were accomplished on a Bio-Basic AX column (2.1 × 20 mm, 5 μm, Waltham, MA). The sample chamber in the autosampler was maintained at 4 °C, and the column was kept at room temperature. The mobile phase consisted of 25 mM ammonium bicarbonate in water (A) and acetonitrile with 0.1% ammonium hydroxide (B) and was delivered at 1 ml/min. The gradient started at 85% of B for 0.2 min, proceeded linearly to 5% of B at 1.2 min, stayed until 2 min, then returned to initial condition at 2.2 min. The total run time was 2.5 min.

Statistics—All average results are presented as mean ± S.E. *p* values were calculated using a two-tailed *t* test. Statistics for gene expression analysis are described above.

RESULTS

Clinically Relevant IDH1/2 Mutations Lead to Nonequivalent Levels of Intracellular 2-HG—We hypothesized that studying the effects of IDH1/2 mutations within their endogenous genomic context would be a well controlled means to examine their oncogenic effects. To accomplish this, clinically relevant IDH1/2 mutations (*IDH1*, R132H and R132C; *IDH2*, R172K and R140Q) were heterozygously inserted into IDH1/2 wild-type HCT116 colorectal cancer cells via homologous recombination with recombinant adeno-associated virus targeting vectors (36). Two isogenic IDH1/2 wild-type controls were used as follows: first, the HCT116 parental cell line; second, an HCT116 clone that went through the targeting process but did not express the mutant allele (clone 16F8). Heterozygous expression of the relevant mutant alleles was observed in all other clones at the mRNA level (data not shown), and insertion of the mutations did not result in notable changes in total IDH1 or IDH2 protein expression (supplemental Fig. S1*A*). Additionally, an IDH1 R132H-specific antibody (45) confirmed the expression of this mutant protein in the relevant clones (supplemental Fig. S1*A*).

Intracellular levels of 2-HG were increased in all IDH1/2 mutant-expressing cells. Surprisingly, both of the IDH2 R140Q/+ clones showed only a slight elevation in intracellular 2-HG levels (~3-fold over parental or the nonexpressing control) (Fig. 1*A* and supplemental Fig. S1*B*; "low 2-HG" in *red*). The low level of 2-HG in these two cell lines is not likely to be an artifact of clonal selection, as ectopic expression of IDH2 R140Q and IDH2 R172K in HCT116 cells showed a similar trend (supplemental Fig. S1*C*). Dramatic increases in 2-HG were observed in each of the IDH1 R132H/+, IDH1 R132C/+, and IDH2 R172K/+ clones (Fig. 1*A*; "high 2-HG" in *blue*), consistent with what has previously been observed. Thus, heterozygous insertion of IDH1/2 mutations in HCT116 successfully generated heterozygously expressed active mutant enzymes.

High Intracellular 2-HG Correlates with EMT-like Phenotypes—To study the gene expression changes induced by mutant IDH1/2, the IDH1/2 wild-type and mutant HCT116 panels were analyzed using Affymetrix U133 plus 2 microarrays (note: the IDH1 R132C/+ clone 2A9 was not yet made at the time of these analyses, but it was used in all follow-up studies). When analyzed based exclusively on IDH1/2 mutational status (see "Experimental Procedures"), we found that 92 probe sets mapping to 76 unique genes were differentially expressed (supplemental Table S1). Noticeably, both IDH2 R140Q/+ clones showed the weakest gene expression changes in the panel (supplemental Fig. S1*D*), tracking with the lower production of 2-HG. To examine whether 2-HG may be a stronger regulator of gene expression changes than IDH1/2 mutation itself, differentially expressed genes based on "high" *versus* "low" 2-HG levels (clones color-coded in figures as *blue* and *red*, respectively) were also examined, and a total of 345 probe sets mapping to 253 unique genes were differentially expressed in the clones with high 2-HG (Fig. 1*B* and supplemental Table S2). Thus, it appears that 2-HG accumulation is a more potent modifier of gene expression and cellular signaling than is mutant IDH1/2 alone.

The observed 2-HG-dependent gene expression changes were analyzed to discover associations with specific signaling pathways. Comparing the genes that show altered expression based on 2-HG levels (from Fig. 1*B* and supplemental Table S2) against gene sets from the GeneGo Metacore database revealed a number of significantly scoring up-regulated and down-regulated gene sets (Fig. 1*C*). Notable among these were multiple gene sets involved in transcription factor- and miRNA-driven EMT (Fig. 1*C*; EMT pathways highlighted in *yellow*). EMT is a developmental process linked to tumorigenesis through the altered regulation of invasion, metastasis, drug sensitivity, and stem cell-like properties (46). To further determine the validity of EMT as a significant pathway alteration in the high 2-HG-producing cells, the top-ranked genes were also compared with three published EMT gene signatures (40–42). Both the up- and down-regulated genes in the three signatures showed a significant overlap with the 2-HG modulated gene set (Fig. 1, *D* and *E*), providing further confirmation that high 2-HG significantly correlates with an induction of EMT-related gene expression in this cell type.

To validate the findings from the microarray, qRT-PCR and immunoblotting were used to validate a subset of the EMT signature genes. Expression of the epithelial marker E-cadherin was reduced at the mRNA level in the high 2-HG clones, whereas expression of the mesenchymal marker vimentin was increased (Fig. 2, *A* and *B*). In the high 2-HG clones, E-cadherin was also decreased at the protein level, and fibronectin, a mesenchymal marker, was increased (Fig. 2*C*).

EMT often tracks with fibroblast-like alterations in cellular morphology. Microscopic examination of the IDH mutant panel revealed that all clones with high levels of intracellular 2-HG showed reduction of the epithelial "cobblestone" morphology present in the IDH1/2 wild-type parental line and acquisition of a more fibroblast-like morphology (Fig. 2*D*). Neither the low 2-HG clones nor the nonexpressing 16F8 clone displayed these morphological alterations. This suggests that the EMT-like phenotype was due to neither a recombinant adeno-associated virus targeting or integration artifact, nor the clonal selection process but rather to an effect of high levels of

2-HG accumulation. A subset of the clones was also analyzed by immunofluorescence for ZO-1 (a component of intercellular tight junctions) and β-catenin (a subunit of the cadherin complex) (46). Corresponding with the epithelial morphology observed, the low 2-HG clones showed β-catenin and ZO-1 staining at the cell membrane and at locations of cell-cell inter-

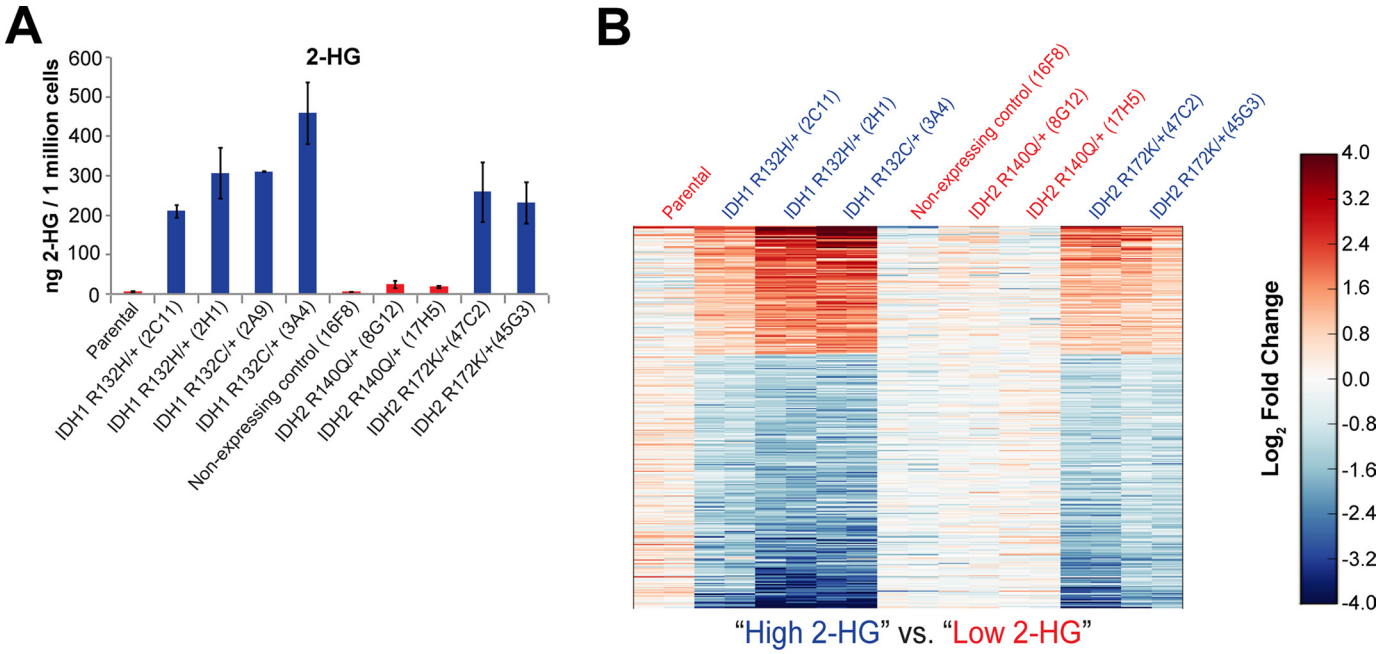

C

		BH corrected p-value	Matches	Number Matched	Category Size
Up	CREB1 activation	3.56E-02	ADRB2 HAS2 HSPA1B ZEB1 GRPR ROR1 FN1 TGFB2 SPP1 SGK PPARG	11	385
	Development TGF-beta-dependent induction of EMT via SMADs	3.56E-02	FN1 TGFB2 VIM ZEB1	4	34
	TBX2 activation	3.56E-02	TGFB2 HAS2	2	3
	ETS1 activation	3.56E-02	SPP1 ABCB1 NR2F2 CXCR4 ZEB1 AKR1B10 GRPR	7	160
	USF1 activation	3.56E-02	SPP1 TGFB2 THBS1 CXCR4 CEACAM1 CYP1A1	6	112
	LBX1 activation	4.86E-02	TGFB2 ZEB1	2	4
	Development MicroRNA-dependent inhibition of EMT	4.86E-02	TGFB2 ZEB1	2	4
Down	SNAI1 inhibition	3.88E-02	EGR1 RAB25 CLDN7 CLDN3 CDH1	5	33
	CEBPB activation	3.88E-02	TRIB3 CYP24A1 INHBE KLRC3 PLAC1 ATF3 ITGAX PDE4D ABCC2 EGR1 IL1RN	11	203

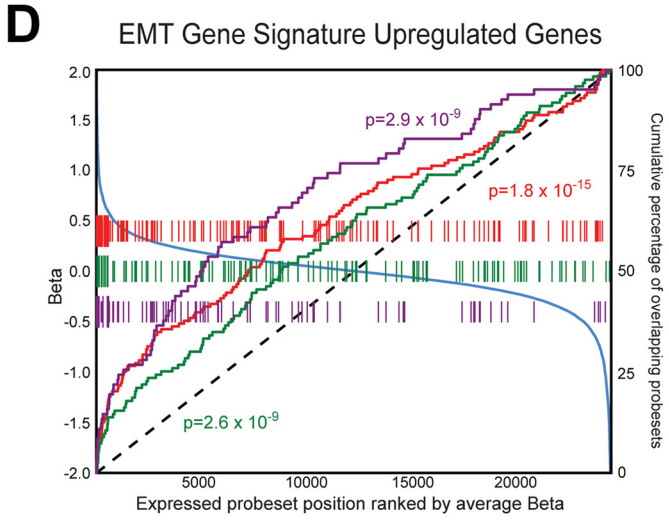

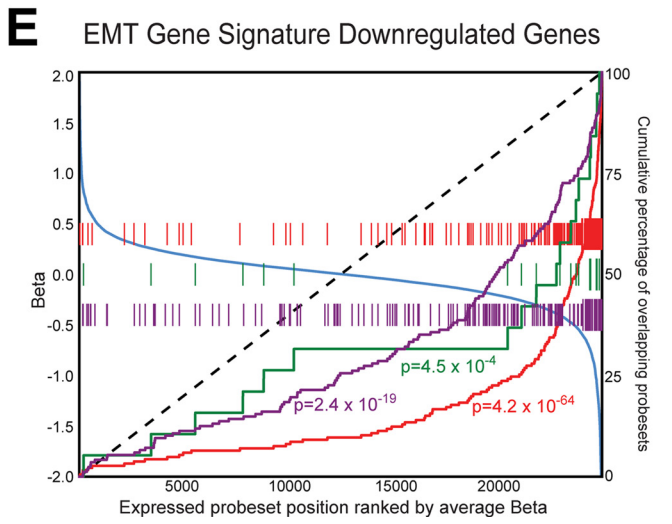

actions, whereas the high 2-HG clones, with a more mesenchymal morphology, showed more diffuse staining for both markers (Fig. 2*E* and supplemental Fig. S2*A*).

To ensure that these EMT phenotypes were not unique to HCT116 cells, IDH1 was similarly mutated to R132H/+ via homologous recombination in the MCF-10A cell line, an immortalized nontumorigenic mammary epithelial cell line, and three independent clones were analyzed. As with HCT116, this approach generated clones that heterozygously expressed mutant IDH1 and produced high levels of 2-HG (Fig. 2*E* and data not shown). IDH1 R132H mutant MCF-10A clones developed many of the same EMT-like phenotypes seen in the high 2-HG HCT116 clones, including a reduction of E-cadherin, increased fibronectin, vimentin, and N-cadherin and an altered and more fibroblast-like morphology (Fig. 2, *F* and *G*, and supplemental Fig. S2, *B*–*C*). Together, these data suggest that high levels of 2-HG production via mutant IDH are sufficient to induce aspects of EMT in different epithelial cell backgrounds.

2-HG Correlates with Increased ZEB1/2 Expression and Decreased miR-200 Expression—The EMT process can be coordinated by any one of a small number of specific transcription factors (46). The expression of ZEB1, a well characterized driver of EMT, tracked closely with high 2-HG levels (Fig. 1*C* and supplemental Table S2). ZEB1 up-regulation was confirmed by both qRT-PCR and immunoblotting (Fig. 3, *A* and *B*). Expression of Slug and Snail, two additional key drivers of EMT, were not correlated with 2-HG levels (data not shown), whereas ZEB2, a paralog of ZEB1, was also generally up-regulated in the high 2-HG clones (Fig. 3*C*). Additionally, ZEB1 and ZEB2 showed increased expression in the IDH1 R132H/+ MCF-10A cells (supplemental Fig. S3, *A*–*C*).

ZEB1 expression is regulated by a number of signaling pathways, including positive regulation via transforming growth factor β signaling and down-regulation by the miR-200 family of microRNAs (miRNA) (47–53). Notably, one of the down-regulated EMT-related pathways enriched in the high 2-HG clones is a "microRNA-dependent inhibition of EMT" (Fig. 1*C*), suggesting a role for miRNAs in altered EMT. To address whether altered mRNA expression was present in the high 2-HG clones, we analyzed expression of the miR-200 family members, miR-200b and miR-200c, in the HCT116 panel. These miRNAs were indeed decreased in the high 2-HG HCT116 clones (Fig. 3, *D* and *E*). In addition, miR-200b and miR-200c both showed down-regulation in MCF-10A cells with IDH1 mutation (supplemental Fig. S3, *D* and *E*). The expression levels of ZEB1, miR-200b, and miR-200c in HCT116 cells were linearly correlated with intracellular 2-HG levels (Fig. 3*F*) suggesting a tight link between 2-HG levels and the expression of these genes.

2-HG Is Sufficient to Cause an EMT-like Phenotype—The above data suggest that 2-HG accumulation is sufficient to induce EMT-like phenotypes via altered ZEB1 and miR-200 family signaling. To determine whether 2-HG is sufficient to modulate expression of this pathway in the absence of IDH1/2 mutation, the levels of ZEB1/2, vimentin, miR-200b/c, and fibronectin were examined in HCT116 parental cells treated with exogenous 2-HG. Sustained exposure to exogenous 2-HG generated intracellular levels that were comparable with those observed in IDH1/2 mutant cells (Fig. 4*A*). At many of the time points examined, 2-HG exposure increased expression of ZEB1/2, vimentin, and fibronectin and decreased expression of miR-200b/c, consistent with our observations in the IDH1/2 mutant high 2-HG clones (Fig. 4, *B*–*G*). E-cadherin expression was not reduced by day 31; however, treatment with 2-HG for 39–74 days did lead to a decrease in E-cadherin levels (Fig. 4*H*). In addition, sustained exposure to 2-HG over time caused a more fibroblast-like morphology, albeit more subtly than the morphology changes observed in the IDH1/2 mutant high 2-HG clones (Fig. 4*I*). This demonstrates that 2-HG exposure alone is sufficient to recapitulate many aspects of the EMT-like phenotypes induced by IDH1/2 mutations in HCT116 cells.

Altered Regulations of ZEB1 and miR-200 Are Necessary for 2-HG-mediated Induction of EMT-like Phenotypes—To address whether ZEB1 up-regulation is necessary for maintenance of the 2-HG-dependent EMT-like phenotypes, we utilized three independent small interfering RNAs (siRNA) to reduce expression of ZEB1 (ZEB1 siRNA A, B, or C) in three separate high level 2-HG HCT116 clones. All ZEB1 siRNAs robustly decreased ZEB1 expression at both the mRNA and protein levels relative to a nontargeting control (NTC) siRNA (Fig. 5*A* and supplemental Fig. S4*A*). ZEB1 knockdown increased E-cadherin protein (Fig. 5*A*) and mRNA (supplemental Fig. S4*B*) and led to a decrease in vimentin and ZEB2 mRNA (supplemental Fig. S4, *C* and *D*), in each of the three clones tested. In addition, ZEB1 knockdown attenuated aspects of mesenchymal morphology, and these cells adopted a more epithelial, cobblestone-like morphology similar to the IDH1/2 wild-type parental clone (Fig. 5*B*).

Next, to examine whether 2-HG-mediated down-regulation of miR-200 is also necessary to cause the EMT-like phenotype, miRNA mimetics were utilized to restore high expression of miR-200b or miR-200c in IDH1/2 mutant HCT116. Addition of either of the miR-200 family members reduced ZEB1 protein

FIGURE 1. **Clinically relevant IDH1/2 mutations lead to nonequivalent levels of intracellular 2-HG and high 2-HG correlates with an EMT signature.** *A,* intracellular 2-HG levels normalized to cell number. Data presented are the average of three or more independent replicates, and *errors bars* represent standard error. *Red,* "low 2-HG"; *blue,* "high 2-HG." *B,* heat map for the 345 probe sets that are differentially expressed in the high 2-HG *versus* low 2-HG clones. Log fold-changes shown are relative to the average of the low 2-HG clones. *Columns* represent HCT116 clones (in duplicate), and *rows* are individual probes. *C,* GeneGo pathway categories altered in the high 2-HG clones ranked by *p* value; only pathways with a corrected *p* value less than 0.05 are shown. *Yellow* highlights observed EMT pathways. *D* and *E,* correlation between three EMT gene signatures (40–42), up-regulated genes (*D*) and down-regulated genes (*E*), in comparison with the top-ranked genes in the high level 2-HG *versus* low level 2-HG data set. *Blue line* represents expressed probe set position and is ranked by average fold-change. The gene sets are color-coded to published EMT datasets as follows: *green* (41); *purple* (40); and *red* (42). The *lines* indicate where the probe sets mapping to genes in the EMT gene signatures appear in our dataset; *taller lines* indicate those genes with a fold-change of at least 1.5 and a nominal *p* value less than 0.05. The *curves* shows the cumulative sum of the probe sets in each of the EMT gene signatures that overlap with our gene list, and the *dashed line* represents the hypothetical cumulative sum for a random list of genes that are unenriched. The *p* values shown are based on a two-tailed Fisher's exact test as described under "Experimental Procedures."

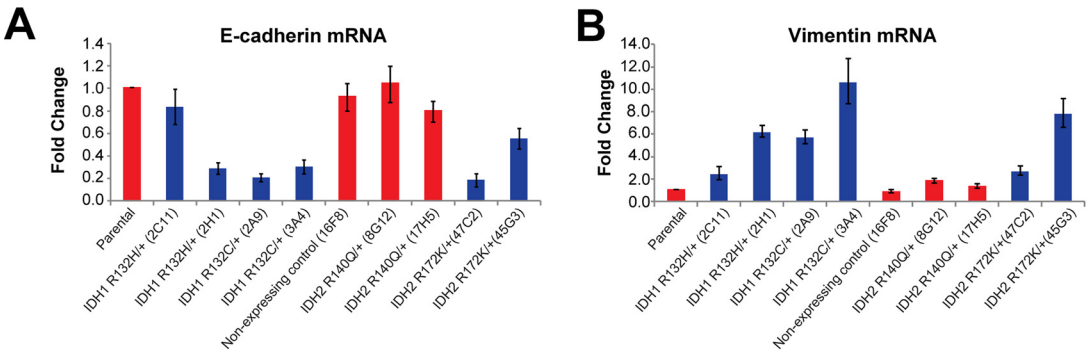
A
E-cadherin mRNA
Fold Change
1.4
1.2
1.0
0.8
0.6
0.4
0.2
0.0
Parental
IDH1 R132H/+ (2C11)
IDH1 R132H/+ (2H1)
IDH1 R132C/+ (2A9)
IDH1 R132C/+ (3A4)
Non-expressing control (16F8)
IDH2 R140Q/+ (8G12)
IDH2 R140Q/+ (17H5)
IDH2 R172K/+(47C2)
IDH2 R172K/+(45G3)
B
Vimentin mRNA
Fold Change
14.0
12.0
10.0
8.0
6.0
4.0
2.0
0.0
Parental
IDH1 R132H/+ (2C11)
IDH1 R132H/+ (2H1)
IDH1 R132C/+ (2A9)
IDH1 R132C/+ (3A4)
Non-expressing control (16F8)
IDH2 R140Q/+ (8G12)
IDH2 R140Q/+ (17H5)
IDH2 R172K/+(47C2)
IDH2 R172K/+(45G3)

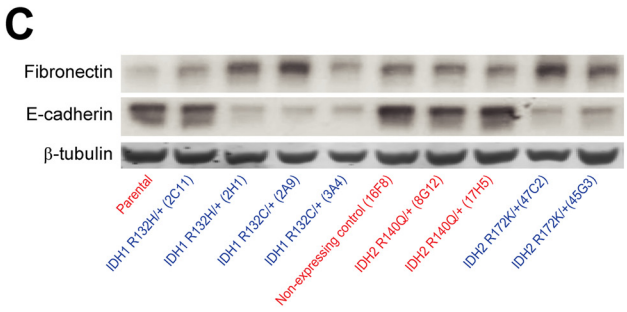
C
Fibronectin
E-cadherin
β-tubulin
Parental
IDH1 R132H/+ (2C11)
IDH1 R132H/+ (2H1)
IDH1 R132C/+ (2A9)
IDH1 R132C/+ (3A4)
Non-expressing control (16F8)
IDH2 R140Q/+ (8G12)
IDH2 R140Q/+ (17H5)
IDH2 R172K/+(47C2)
IDH2 R172K/+(45G3)

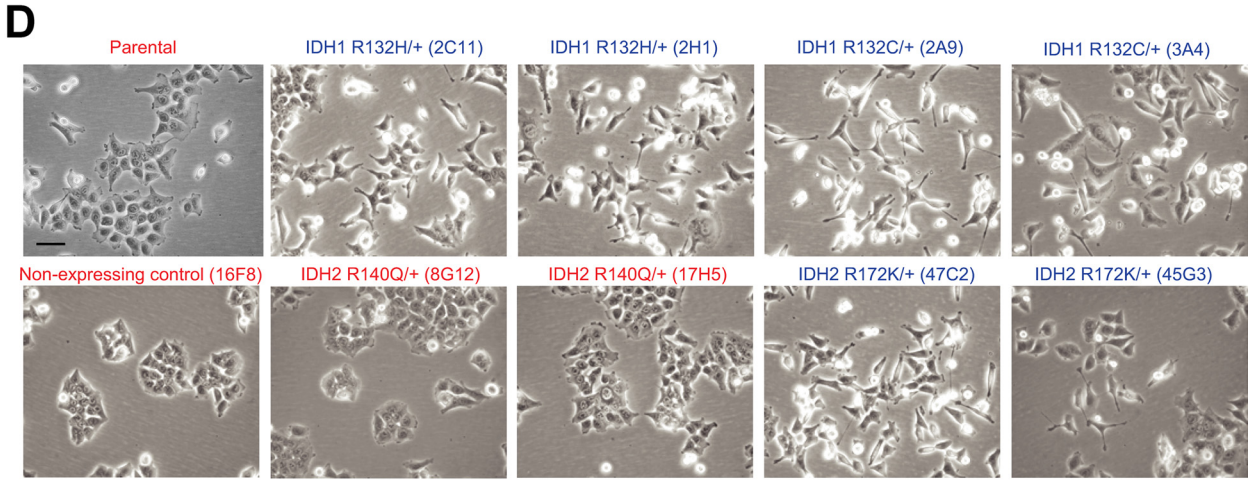
D
Parental
IDH1 R132H/+ (2C11)
IDH1 R132H/+ (2H1)
IDH1 R132C/+ (2A9)
IDH1 R132C/+ (3A4)
Non-expressing control (16F8)
IDH2 R140Q/+ (8G12)
IDH2 R140Q/+ (17H5)
IDH2 R172K/+ (47C2)
IDH2 R172K/+ (45G3)

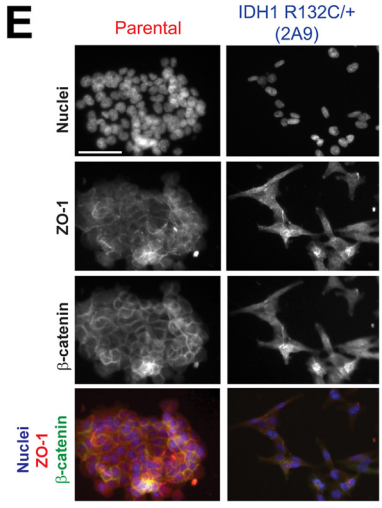
E
Parental
IDH1 R132C/+ (2A9)
Nuclei
ZO-1
β-catenin
Nuclei
ZO-1
β-catenin

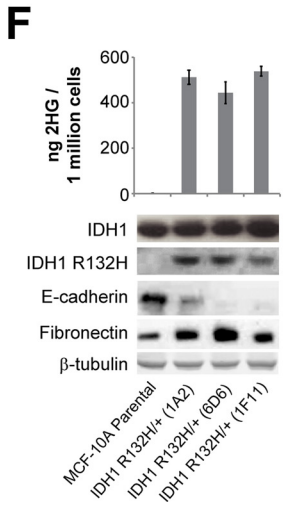
F
ng 2HG / 1 million cells
600
400
200
0
IDH1
IDH1 R132H
E-cadherin
Fibronectin
β-tubulin
MCF-10A Parental
IDH1 R132H/+ (1A2)
IDH1 R132H/+ (6D6)
IDH1 R132H/+ (1F11)

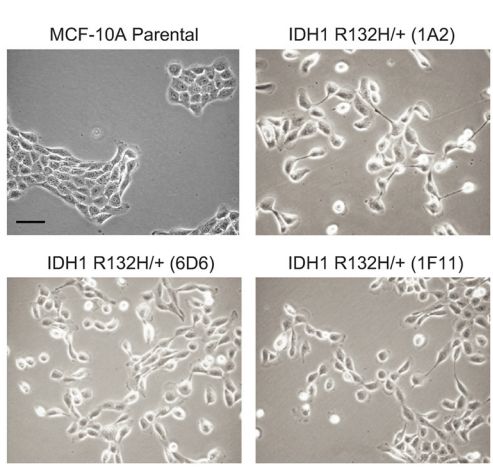
G
MCF-10A Parental
IDH1 R132H/+ (1A2)
IDH1 R132H/+ (6D6)
IDH1 R132H/+ (1F11)

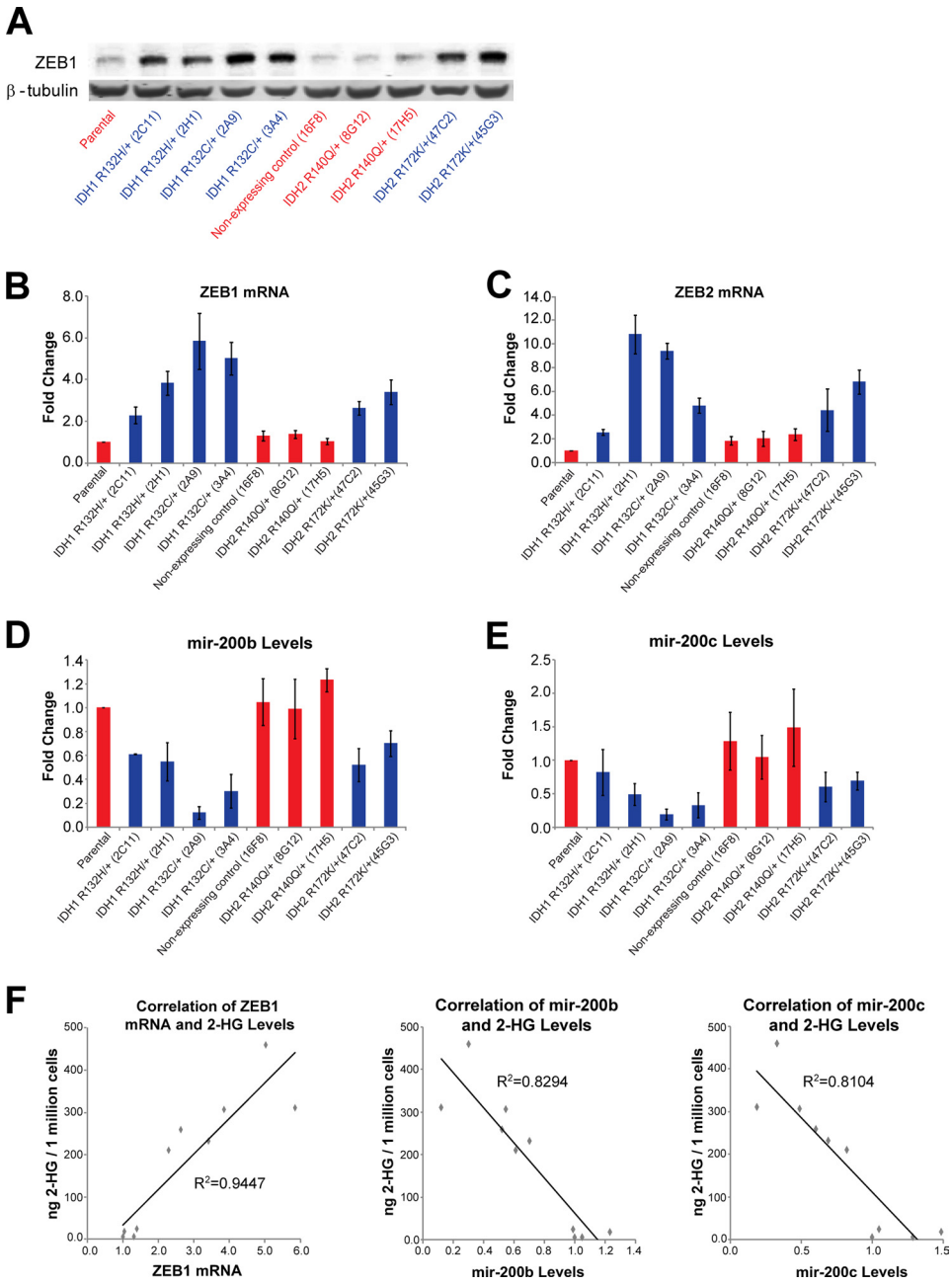

FIGURE 3. **2-HG correlates with increased ZEB1 and decreased miR-200 expression.** *A*, Western blot of HCT116 parental and IDH1/2 mutant clones analyzed by immunoblotting for the indicated proteins. *B* and *C*, ZEB1 (*B*) and ZEB2 (*C*) mRNA levels in the HCT116 parental and IDH1/2 mutant clones. *D* and *E*, miR-200b (*D*) and miR-200c (*E*) levels in the HCT116 parental and IDH1/2 mutant clones. Levels are normalized to RNU44. *F*, linear correlation of ZEB1 (data from *B*), miR-200b (data from *D*), and miR-200c (data from *E*) RNA levels to 2-HG intracellular levels (data from Fig. 1*A*). *Blue*, HCT116 clones with high intracellular levels of 2-HG; *red*, HCT116 clones with low intracellular levels of 2-HG.

and mRNA levels, increased E-cadherin protein and mRNA, and decreased levels of vimentin and ZEB2 mRNA (Fig. 5*C* and supplemental Fig. S4*E*). Additionally, the miRNA mimetics induced morphology changes similar to those seen with ZEB1 siRNA, leading to a more epithelial morphology (Fig. 5*D*). Together, these data demonstrate that signaling through miR-200 and ZEB1 is necessary for EMT-like phenotypes caused by mutant IDH1/2 and 2-HG.

FIGURE 2. **High intracellular 2-HG correlates with EMT-like phenotypes.** *A* and *B*, E-cadherin (*A*) and vimentin (*B*) mRNA levels in the HCT116 parental and IDH1/2 mutant clones, as measured by qRT-PCR. Data presented are the average of three or more independent replicates normalized to β_2-microglobulin expression, relative to the parental clone. *Errors bars* represent standard error. Unless otherwise noted, all mRNA data are presented in this manner. *C*, Western blot of HCT116 parental and IDH1/2 mutant clones analyzed by immunoblotting for the indicated proteins. *D*, representative microscopy images of the HCT116 parental and IDH1/2 mutant cells. *Scale bar*, 50 μm. *E*, immunofluorescence images of HCT116 parental and HCT116 IDH1 R132C/+ (2A9) clones stained with ZO-1 and β-catenin. *F, upper panel*, intracellular 2-HG levels of MCF-10A parental and IDH1 R132H/+ mutants. Data are presented as in Fig. 1*A*. *Lower panel*, Western blot of MCF-10A parental and IDH1 R132H/+ mutants analyzed by immunoblotting for the indicated proteins. *G*, representative images of the MCF-10A parental and IDH1 R132H/+ clones. *Scale bar*, 50 μm. *Blue*, HCT116 clones with high intracellular levels of 2-HG; *red*, HCT116 clones with low intracellular levels of 2-HG.

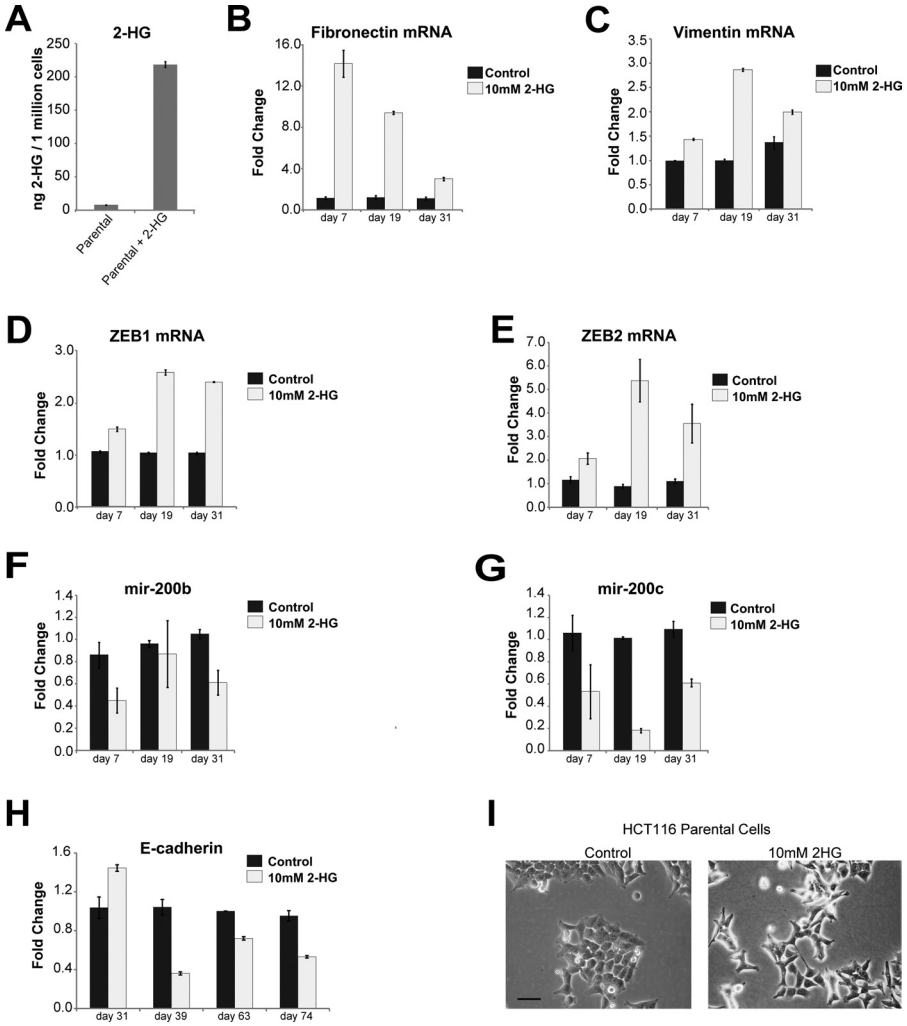

FIGURE 4. **2-HG is sufficient to cause an EMT-like phenotype.** *A,* intracellular 2-HG levels of HCT116 parental cells grown in the absence or presence of 10 mM 2-HG for 7 days. *B–H,* qRT-PCR measurement of RNA levels for the indicated transcripts in HCT116 parental cells grown in the absence or presence of 10 mM 2-HG for the indicated number of days. For each time point, data are normalized to the untreated control. *I,* representative images of HCT116 parental cells grown in the absence or presence of 10 mM 2-HG for 31 days. *Scale bar,* 50 μm.

EMT-like Phenotypes in IDH1 Mutant Cells Are Reversible by IDH1 Knockdown—ZEB1 and miR-200 regulate each other in a double-negative feedback loop to promote either an epithelial or mesenchymal phenotype (54). Although 2-HG shifts this loop toward a ZEB1 high/mesenchymal phenotype, it is unclear if blocking 2-HG accumulation via IDH inhibition would allow for cells to switch back to a more epithelial phenotype. To address this question, RNA interference was used to reduce expression of IDH1. The IDH1 R132H/+ 2H1 clone was transduced with two independent doxycycline-inducible shRNAs against IDH1 (or a nontargeting control shRNA). Upon doxycycline exposure, IDH1 protein and mRNA levels rapidly and robustly decreased, and 2-HG levels were greatly reduced after 48 h (Fig. 6, *A* and *B*). Unlike the case with ZEB1 knockdown or addition of the miR-200 mimetics, changes in EMT markers were not initially observed upon IDH1 knockdown, despite the reduction of 2-HG (Fig. 6, *B* and *C*). However, after prolonged (12 days) IDH1 knockdown, decreased fibronectin, vimentin, ZEB1 and ZEB2, and increased miR-200b and miR-200c were observed. Restoration of E-cadherin expression was most reticent to change and was not up-regulated with kinetics similar to miR-200b and miR-200c. (Fig. 6*D*). Consistent with the observed changes in EMT marker expression, prolonged IDH1 knockdown also partially reversed the fibroblast-like morphology (Fig. 6*E*). These results demonstrate that continued expression of mutant IDH1 is required to maintain mesenchymal phenotypes in these cells and indicate that mutant IDH-dependent phenotypes are reversible.

DISCUSSION

Despite the high prevalence of IDH1 and IDH2 mutations in a wide variety of cancers, the lack of IDH1/2 mutant cell line models has made it challenging to elucidate the function of these oncogenes in tumorigenesis and to confirm whether phenotypes induced by mutant IDH are indeed reversible after their establishment. This question is critical in light of the discovery that some cancer-causing mutations may not be continuously required in established tumors (55). Using the IDH1/2 isogenic epithelial cell models reported herein, we note an unexpected difference in the ability of at least one clinically recurrent IDH2 mutation, R140Q, to produce 2-HG. From this, we show that high intracellular 2-HG accumulation, but not

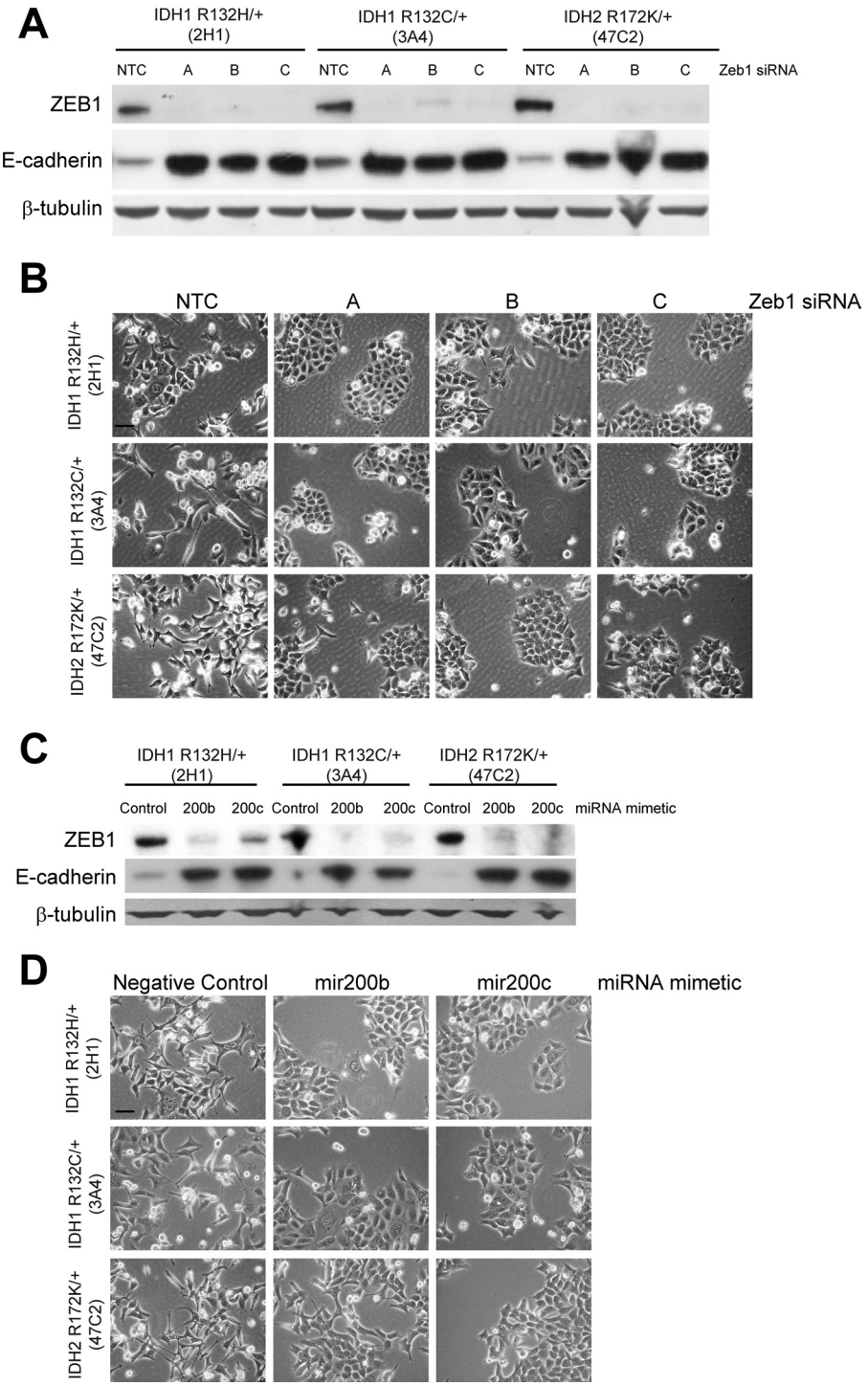

FIGURE 5. **Altered regulation of ZEB1 and miR-200 are required for 2-HG-mediated induction of EMT-like phenotypes.** *A,* Western blot of HCT116 IDH1 R132H/+ clone 2H1, HCT116 IDH1 R132C/+ clone 3A4, and HCT116 IDH2 R172K/+ clone 47C2 transfected with NTC siRNAs or one of three siRNAs targeting ZEB1 (A, B, or C) for 72 h. *B,* representative images of cells treated as in *A* are shown. *Scale bar,* 50 μm. *C,* Western blot of HCT116 IDH1 R132H/+ clone 2H1, HCT116 IDH1 R132C/+ clone 3A4, and HCT116 IDH2 R172K/+ clone 47C2 transfected with the indicated miRNA mimetics for 72. *D,* representative images from cells treated as in *C*. *Scale bar,* 50 μm.

necessarily IDH1/2 mutations themselves, leads to an EMT-like phenotype characterized by both morphological and gene expression changes. Consistent with this finding, we observe that exogenous 2-HG exposure is sufficient to generate EMT-like phenotypes in IDH1/2 wild-type cells. ZEB1 up-regulation and miR-200 down-regulation are both required to mediate mutant IDH1/2-dependent EMT-like behavior in HCT116 cells, as either ZEB1 knockdown or restoration of high expression of miR-200 revert this phenotype. Importantly, continued mutant IDH1 expression is also required for EMT-like behaviors, as knockdown of IDH1 in an IDH1 R132H/+ mutant clone reverts cells to a more epithelial-like phenotype. Thus, these results identify specific signaling changes induced by IDH1/2 mutation and 2-HG that act through a specific transcription

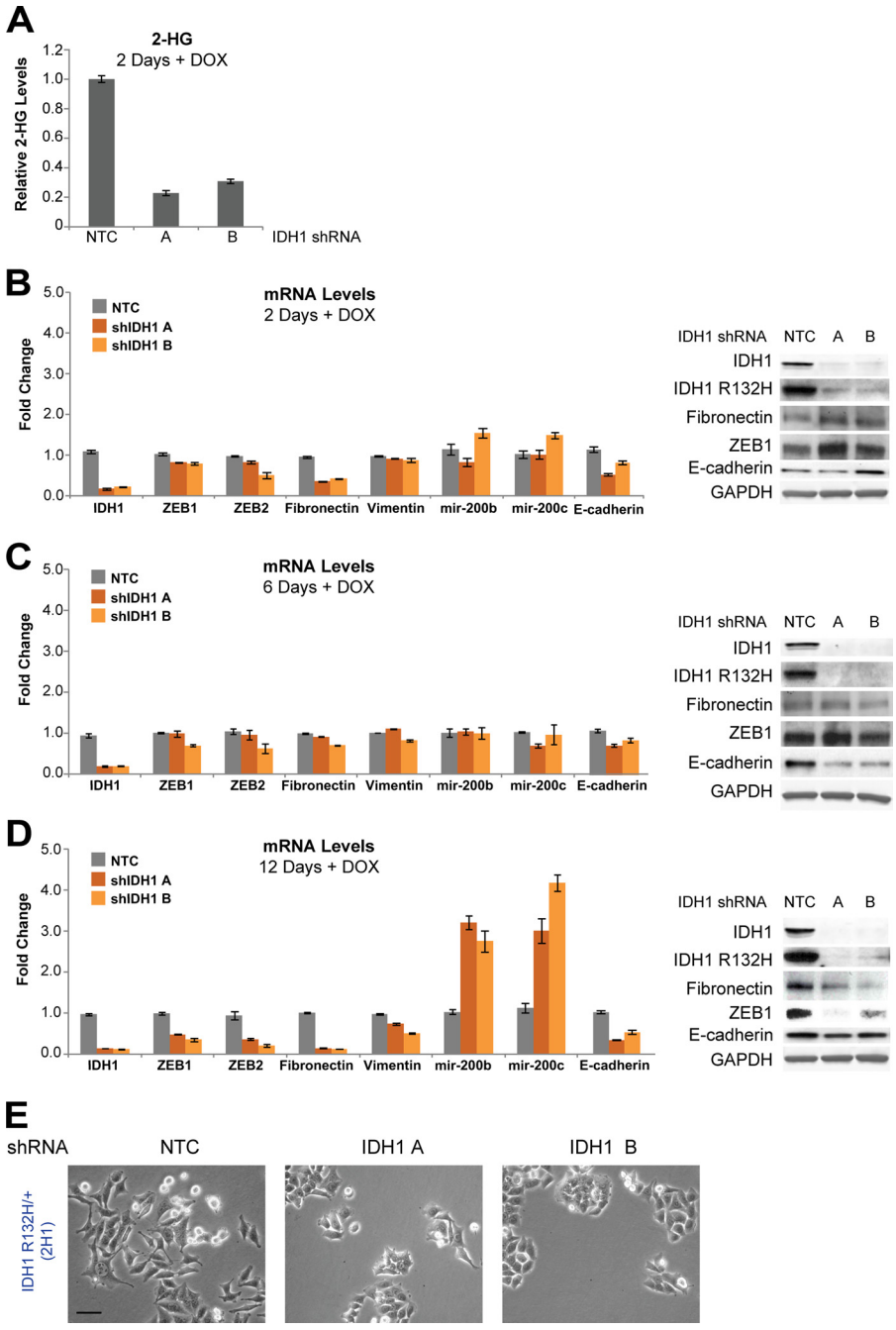

FIGURE 6. **Mutant IDH1/2-induced EMT-like phenotype is reversible and dependent on IDH1/2 expression.** *A,* intracellular 2-HG levels of HCT116 IDH1 R132H/+ clone 2H1 cells transduced with two doxycycline-inducible shRNAs targeting IDH1 or an NTC. Cells were treated with doxycycline for 2 days. 2-HG levels are normalized to NTC. *B–D,* qRT-PCR measurement of mRNA levels (*left panel*) and Western blot analysis (*right panel*) of HCT116 IDH1 R132H/+ clone 2H1 cells transduced with two doxycycline-inducible shRNAs targeting IDH1 or NTC. Cells were treated with doxycycline for 2 (*B*), 6 (*C*), or 12 (*D*) days. *E,* representative images of cells treated as in *D*. *Scale bar,* 50 μm.

factor (ZEB1). Moreover, we show that it is possible to reverse this mutant IDH-induced phenotype through direct modulation of IDH1. To our knowledge, this is the first study to demonstrate that mutant IDH and 2-HG accumulation generate *reversible* signaling changes that act through discrete pathways. With the promise of IDH inhibitors on the horizon (19, 56), these data suggest the exciting possibility that inhibition of mutant IDH function will indeed be able to reverse the downstream signaling effects initiated by IDH1/2 mutations in clinically observed cancers.

Reversibility of Mutant IDH Phenotypes—Recent data suggest that mutant IDH-dependent phenotypes can take a considerable amount of time to develop; an IDH mutant mouse knock-in model has a long latency (32), and *in vitro*, mutant IDH overexpression models appear to require extended periods in culture before robust phenotypes emerge (25, 26, 34). In particular, multiple lines of evidence have established that mutant IDH and 2-HG generate genome-wide increases in DNA methylation (11, 32, 34, 57), an epigenetic change that can be stable over many cell divisions, even in the absence of the initiating

stimulus (58). This raises an obvious question pertinent to the development of therapeutics. Are mutant IDH-dependent phenotypes reversible? If so, how long will it take for mutant IDH inhibition to modulate these downstream pathways? Although we observe that ZEB1 knockdown or restoration of high expression of miR-200 rapidly reverses many aspects of the 2-HG-dependent EMT phenotype (within 72 h), the effect of IDH1 knockdown on reverting this phenotype was comparatively delayed, with consistent reversion of EMT behaviors observed only after 12 days of continuous IDH1 knockdown. This was despite the fact that IDH1 knockdown robustly lowered IDH1 protein and 2-HG levels within 48 h.

Such delays in the reversibility of the mutant IDH EMT-like phenotype are consistent with the hypothesis that mutant IDH acts through modulation of epigenetic marks. Mutant IDH has been linked to changes in both histone and DNA methylation, and 2-HG has been shown to be sufficient to inhibit enzymes involved in epigenetic modulation (24, 26–30, 32). These epigenetic changes may not be prone to rapid turnover (58), and this could explain the delay in reversion of the EMT phenotype that we observe. If these findings can be extended to clinically observed tumors, they suggest that rapid responses to mutant IDH inhibition may not necessarily occur but that perseverance with IDH inhibition over time to continually lower 2-HG levels may ultimately demonstrate efficacy. It will be important to confirm such findings in a wider variety of preclinical models and ultimately in the clinic.

Mutant IDH-induced EMT in Tumorigenesis—Ample evidence suggests that the EMT process is involved in tumorigenesis and contributes to invasion, metastasis, and drug resistance (46, 59). In particular, there have been a number of reports that provide strong evidence linking the acquisition of an EMT phenotype to promotion of a more stem-like cell (60). Thus, the attenuation of epithelial characteristics in HCT116 and MCF-10A cells is consistent with an emerging theme that mutant IDH and 2-HG are able to block aspects of cellular differentiation and promote progenitor-like phenotypes (26, 30, 32).

Although mutations in IDH1/2 are commonly found outside of epithelial lineages, 10–23% of intrahepatic cholangiocarcinomas, a cancer of bile duct epithelium, have recurrent mutations in IDH1/2 (10, 11), and IDH1/2 mutations have been reported, albeit rarely, in lung, prostate, and colon tumors (12–16). This raises the possibility that mutant IDH1/2- and 2-HG-mediated EMT may play a role in the pathology of these epithelial tumors, with cholangiocarcinoma in particular. Notably, a recent study finds that a subset of intrahepatic cholangiocarcinoma exhibit aspects of EMT, with miR-200c reduction as a central phenotype (61). It will be intriguing to determine whether IDH mutations track with this subtype of cholangiocarcinoma.

2-HG Drives Specific Changes in Gene Expression—The use of genetically matched IDH1/2 heterozygous mutant and wild-type cell lines allowed for the elucidation of phenotypic differences among clinically relevant IDH1/2 mutations. IDH2 R140Q mutation, but not IDH2 R172K mutation, resulted in a surprisingly subtle increase in the levels of intracellular 2-HG, and it had the weakest effects on gene expression modulation. This suggests that although IDH2 Arg-140 mutations are clearly associated with 2-HG production and AML, they could potentially drive relatively weaker phenotypes than other IDH1/2 mutations or have a longer latency period. Observations of 2-HG levels in IDH2 Arg-140 mutant AML suggest that these mutations may indeed produce relatively less 2-HG than other IDH mutations (6, 8, 62), and an additional study suggests AML patients with IDH2 Arg-140 mutations are diagnosed at a significantly older age than are patients with Arg-172 mutations (63). Given these observed differences, and the variation in prevalence of IDH1 *versus* IDH2 mutations in different tumor types, we speculate that there may be key differences in how specific mutations in IDH1 or IDH2 affect cellular biology. Analysis of outcomes in a larger cohort of patients with different IDH1/2 mutations will be needed to further validate the relevance of these findings.

As the common phenotype of IDH1/2 mutant tumors is accumulation of the oncometabolite 2-HG (6, 8, 20, 62), we focused this study on the effects of high levels of 2-HG accumulation rather than IDH1/2 mutation itself; the data herein demonstrate that 2-HG accumulation via mutant IDH proteins is sufficient to cause dramatic effects on gene expression. Given the previously described ability of mutant IDH to cause broad genome-wide epigenetic changes (26, 30, 32), it was surprising that different IDH1/2 mutations (with high 2-HG production) exerted common signaling effects on a specific pathway, ZEB1/miR-200 regulated EMT, in both colon and breast epithelial lines. We speculate that the altered regulation of some signaling pathways (perhaps through differential sensitivity to epigenetic changes affecting expression) is more sensitive to 2-HG levels. In particular, it will be interesting to determine whether signaling loops regulating cell behavior, such as the ZEB1/miR-200 loop, are particularly sensitive to 2-HG-dependent perturbations. A growing number of miRNA/transcription factor pairs have been identified that regulate cell phenotypes in a manner similar to ZEB1/miR-200 (64–66). A deeper mechanistic understanding of how 2-HG affects a change in ZEB1/miR-200 signaling in HCT116 and MCF-10A cells could elucidate common mechanisms of 2-HG oncometabolite function in a wider variety of tissue types.

Acknowledgments—We thank Ming Xu and Julie Downall for technical assistance. We thank Markus Warmuth, Peter Finan, Chris Torrance, Darrin Disley, Christine Schofield, Jeremy Ahouse, Alan Buckler, Marjorie Lechevalier, Liz Leveille, Alexandra Rieck, Kamila Pytel, Rachael Leah, Hatice Akarsu, Jane Elliott, Ramu Mangena, Mark Stockdale, Claire Mahoney, and Alessia Mira for assistance with generation of the isogenic cell lines. We thank Jinyun Chen, Franklin Chung, Nika Danial, Brant Firestone, Pascal Fortin, Aron Jaffe, Heather Keane, Nicholas Keen, Neil Kubica, Margaret McLaughlin, Rosa Ng, Dale Porter, William Sellers, KellyAnn Sheppard, Kelly Slocum, Frank Stegmeier, Charles Stiles, German Velez-Reyes, Steve Woolfenden, Wenlai Zhou, Suzanne Zhu, and the Novartis post-doctoral fellows for helpful discussions of this work.

REFERENCES

1. Arai, M., Nobusawa, S., Ikota, H., Takemura, S., and Nakazato, Y. (2012) Frequent IDH1/2 mutations in intracranial chondrosarcoma: a possible

diagnostic clue for its differentiation from chordoma. *Brain Tumor Pathol.* 1–6

2. Cairns, R. A., Iqbal, J., Lemonnier, F., Kucuk, C., de Leval, L., Jais, J. P., Parrens, M., Martin, A., Xerri, L., Brousset, P., Chan, L. C., Chan, W. C., Gaulard, P., and Mak, T. W. (2012) IDH2 mutations are frequent in angioimmunoblastic T-cell lymphoma. *Blood* **119,** 1901–1903
3. Hayden, J. T., Frühwald, M. C., Hasselblatt, M., Ellison, D. W., Bailey, S., and Clifford, S. C. (2009) Frequent IDH1 mutations in supratentorial primitive neuroectodermal tumors (sPNET) of adults but not children. *Cell Cycle* **8,** 1806–1807
4. Parsons, D. W., Jones, S., Zhang, X., Lin, J. C., Leary, R. J., Angenendt, P., Mankoo, P., Carter, H., Siu, I. M., Gallia, G. L., Olivi, A., McLendon, R., Rasheed, B. A., Keir, S., Nikolskaya, T., Nikolsky, Y., Busam, D. A., Tekleab, H., Diaz, L. A., Jr., Hartigan, J., Smith, D. R., Strausberg, R. L., Marie, S. K., Shinjo, S. M., Yan, H., Riggins, G. J., Bigner, D. D., Karchin, R., Papadopoulos, N., Parmigiani, G., Vogelstein, B., Velculescu, V. E., and Kinzler, K. W. (2008) An integrated genomic analysis of human glioblastoma multiforme. *Science* **321,** 1807–1812
5. Yan, H., Parsons, D. W., Jin, G., McLendon, R., Rasheed, B. A., Yuan, W., Kos, I., Batinic-Haberle, I., Jones, S., Riggins, G. J., Friedman, H., Friedman, A., Reardon, D., Herndon, J., Kinzler, K. W., Velculescu, V. E., Vogelstein, B., and Bigner, D. D. (2009) IDH1 and IDH2 mutations in gliomas. *N. Engl. J. Med.* **360,** 765–773
6. Ward, P. S., Patel, J., Wise, D. R., Abdel-Wahab, O., Bennett, B. D., Coller, H. A., Cross, J. R., Fantin, V. R., Hedvat, C. V., Perl, A. E., Rabinowitz, J. D., Carroll, M., Su, S. M., Sharp, K. A., Levine, R. L., and Thompson, C. B. (2010) The common feature of leukemia-associated IDH1 and IDH2 mutations is a neomorphic enzyme activity converting α-ketoglutarate to 2-hydroxyglutarate. *Cancer Cell* **17,** 225–234
7. Mardis, E. R., Ding, L., Dooling, D. J., Larson, D. E., McLellan, M. D., Chen, K., Koboldt, D. C., Fulton, R. S., Delehaunty, K. D., McGrath, S. D., Fulton, L. A., Locke, D. P., Magrini, V. J., Abbott, R. M., Vickery, T. L., Reed, J. S., Robinson, J. S., Wylie, T., Smith, S. M., Carmichael, L., Eldred, J. M., Harris, C. C., Walker, J., Peck, J. B., Du, F., Dukes, A. F., Sanderson, G. E., Brummett, A. M., Clark, E., McMichael, J. F., Meyer, R. J., Schindler, J. K., Pohl, C. S., Wallis, J. W., Shi, X., Lin, L., Schmidt, H., Tang, Y., Haipek, C., Wiechert, M. E., Ivy, J. V., Kalicki, J., Elliott, G., Ries, R. E., Payton, J. E., Westervelt, P., Tomasson, M. H., Watson, M. A., Baty, J., Heath, S., Shannon, W. D., Nagarajan, R., Link, D. C., Walter, M. J., Graubert, T. A., DiPersio, J. F., Wilson, R. K., and Ley, T. J. (2009) Recurring mutations found by sequencing an acute myeloid leukemia genome. *N. Engl. J. Med.* **361,** 1058–1066
8. Gross, S., Cairns, R. A., Minden, M. D., Driggers, E. M., Bittinger, M. A., Jang, H. G., Sasaki, M., Jin, S., Schenkein, D. P., Su, S. M., Dang, L., Fantin, V. R., and Mak, T. W. (2010) Cancer-associated metabolite 2-hydroxyglutarate accumulates in acute myelogenous leukemia with isocitrate dehydrogenase 1 and 2 mutations. *J. Exp. Med.* **207,** 339–344
9. Amary, M. F., Bacsi, K., Maggiani, F., Damato, S., Halai, D., Berisha, F., Pollock, R., O'Donnell, P., Grigoriadis, A., Diss, T., Eskandarpour, M., Presneau, N., Hogendoorn, P. C., Futreal, A., Tirabosco, R., and Flanagan, A. M. (2011) IDH1 and IDH2 mutations are frequent events in central chondrosarcoma and central and periosteal chondromas but not in other mesenchymal tumours. *J. Pathol.* **224,** 334–343
10. Borger, D. R., Tanabe, K. K., Fan, K. C., Lopez, H. U., Fantin, V. R., Straley, K. S., Schenkein, D. P., Hezel, A. F., Ancukiewicz, M., Liebman, H. M., Kwak, E. L., Clark, J. W., Ryan, D. P., Deshpande, V., Dias-Santagata, D., Ellisen, L. W., Zhu, A. X., and Iafrate, A. J. (2012) Frequent mutation of isocitrate dehydrogenase (IDH)1 and IDH2 in cholangiocarcinoma identified through broad-based tumor genotyping. *Oncologist* **17,** 72–79
11. Wang, P., Dong, Q., Zhang, C., Kuan, P. F., Liu, Y., Jeck, W. R., Andersen, J. B., Jiang, W., Savich, G. L., Tan, T. X., Auman, J. T., Hoskins, J. M., Misher, A. D., Moser, C. D., Yourstone, S. M., Kim, J. W., Cibulskis, K., Getz, G., Hunt, H. V., Thorgeirsson, S. S., Roberts, L. R., Ye, D., Guan, K. L., Xiong, Y., Qin, L. X., and Chiang, D. Y. (2012) Mutations in isocitrate dehydrogenase 1 and 2 occur frequently in intrahepatic cholangiocarcinomas and share hypermethylation targets with glioblastomas. *Oncogene* doi: 10.1038/onc.2012.315
12. Lopez, G. Y., Reitman, Z. J., Solomon, D., Waldman, T., Bigner, D. D., McLendon, R. E., Rosenberg, S. A., Samuels, Y., and Yan, H. (2010) IDH1(R132) mutation identified in one human melanoma metastasis but not correlated with metastases to the brain. *Biochem. Biophys. Res. Commun.* **398,** 585–587
13. Ghiam, A. F., Cairns, R. A., Thoms, J., Dal Pra, A., Ahmed, O., Meng, A., Mak, T. W., and Bristow, R. G. (2012) IDH mutation status in prostate cancer. *Oncogene* **31,** 3826
14. Taylor, B. S., Schultz, N., Hieronymus, H., Gopalan, A., Xiao, Y., Carver, B. S., Arora, V. K., Kaushik, P., Cerami, E., Reva, B., Antipin, Y., Mitsiades, N., Landers, T., Dolgalev, I., Major, J. E., Wilson, M., Socci, N. D., Lash, A. E., Heguy, A., Eastham, J. A., Scher, H. I., Reuter, V. E., Scardino, P. T., Sander, C., Sawyers, C. L., and Gerald, W. L. (2010) Integrative genomic profiling of human prostate cancer. *Cancer Cell* **18,** 11–22
15. Kang, M. R., Kim, M. S., Oh, J. E., Kim, Y. R., Song, S. Y., Seo, S. I., Lee, J. Y., Yoo, N. J., and Lee, S. H. (2009) Mutational analysis of IDH1 codon 132 in glioblastomas and other common cancers. *Int. J. Cancer* **125,** 353–355
16. Sequist, L. V., Heist, R. S., Shaw, A. T., Fidias, P., Rosovsky, R., Temel, J. S., Lennes, I. T., Digumarthy, S., Waltman, B. A., Bast, E., Tammireddy, S., Morrissey, L., Muzikansky, A., Goldberg, S. B., Gainor, J., Channick, C. L., Wain, J. C., Gaissert, H., Donahue, D. M., Muniappan, A., Wright, C., Willers, H., Mathisen, D. J., Choi, N. C., Baselga, J., Lynch, T. J., Ellisen, L. W., Mino-Kenudson, M., Lanuti, M., Borger, D. R., Iafrate, A. J., Engelman, J. A., and Dias-Santagata, D. (2011) Implementing multiplexed genotyping of non-small cell lung cancers into routine clinical practice. *Ann. Oncol.* **22,** 2616–2624
17. Sjöblom, T., Jones, S., Wood, L. D., Parsons, D. W., Lin, J., Barber, T. D., Mandelker, D., Leary, R. J., Ptak, J., Silliman, N., Szabo, S., Buckhaults, P., Farrell, C., Meeh, P., Markowitz, S. D., Willis, J., Dawson, D., Willson, J. K., Gazdar, A. F., Hartigan, J., Wu, L., Liu, C., Parmigiani, G., Park, B. H., Bachman, K. E., Papadopoulos, N., Vogelstein, B., Kinzler, K. W., and Velculescu, V. E. (2006) The consensus coding sequences of human breast and colorectal cancers. *Science* **314,** 268–274
18. Dang, L., Jin, S., and Su, S. M. (2010) IDH mutations in glioma and acute myeloid leukemia. *Trends Mol. Med.* **16,** 387–397
19. Yen, K. E., and Schenkein, D. P. (2012) Cancer-associated isocitrate dehydrogenase mutations. *Oncologist* **17,** 5–8
20. Dang, L., White, D. W., Gross, S., Bennett, B. D., Bittinger, M. A., Driggers, E. M., Fantin, V. R., Jang, H. G., Jin, S., Keenan, M. C., Marks, K. M., Prins, R. M., Ward, P. S., Yen, K. E., Liau, L. M., Rabinowitz, J. D., Cantley, L. C., Thompson, C. B., Vander Heiden, M. G., and Su, S. M. (2009) Cancer-associated IDH1 mutations produce 2-hydroxyglutarate. *Nature* **462,** 739–744
21. Struys, E. A., Salomons, G. S., Achouri, Y., Van Schaftingen, E., Grosso, S., Craigen, W. J., Verhoeven, N. M., and Jakobs, C. (2005) Mutations in the D-2-hydroxyglutarate dehydrogenase gene cause D-2-hydroxyglutaric aciduria. *Am. J. Hum. Genet.* **76,** 358–360
22. Kranendijk, M., Struys, E. A., Salomons, G. S., Van der Knaap, M. S., and Jakobs, C. (2012) Progress in understanding 2-hydroxyglutaric acidurias. *J. Inherit. Metab. Dis.* **35,** 571–587
23. Loenarz, C., and Schofield, C. J. (2008) Expanding chemical biology of 2-oxoglutarate oxygenases. *Nat. Chem. Biol.* **4,** 152–156
24. Xu, W., Yang, H., Liu, Y., Yang, Y., Wang, P., Kim, S. H., Ito, S., Yang, C., Wang, P., Xiao, M. T., Liu, L. X., Jiang, W. Q., Liu, J., Zhang, J. Y., Wang, B., Frye, S., Zhang, Y., Xu, Y. H., Lei, Q. Y., Guan, K. L., Zhao, S. M., and Xiong, Y. (2011) Oncometabolite 2-hydroxyglutarate is a competitive inhibitor of α-ketoglutarate-dependent dioxygenases. *Cancer Cell* **19,** 17–30
25. Koivunen, P., Lee, S., Duncan, C. G., Lopez, G., Lu, G., Ramkissoon, S., Losman, J. A., Joensuu, P., Bergmann, U., Gross, S., Travins, J., Weiss, S., Looper, R., Ligon, K. L., Verhaak, R. G., Yan, H., and Kaelin, W. G., Jr. (2012) Transformation by the (*R*)-enantiomer of 2-hydroxyglutarate linked to EGLN activation. *Nature* **483,** 484–488
26. Lu, C., Ward, P. S., Kapoor, G. S., Rohle, D., Turcan, S., Abdel-Wahab, O., Edwards, C. R., Khanin, R., Figueroa, M. E., Melnick, A., Wellen, K. E., O'Rourke, D. M., Berger, S. L., Chan, T. A., Levine, R. L., Mellinghoff, I. K., and Thompson, C. B. (2012) IDH mutation impairs histone demethylation and results in a block to cell differentiation. *Nature* **483,** 474–478
27. Deneberg, S., Guardiola, P., Lennartsson, A., Qu, Y., Gaidzik, V., Blanchet, O., Karimi, M., Bengtzén, S., Nahi, H., Uggla, B., Tidefelt, U., Höglund, M.,

Paul, C., Ekwall, K., Döhner, K., and Lehmann, S. (2011) Prognostic DNA methylation patterns in cytogenetically normal acute myeloid leukemia are predefined by stem cell chromatin marks. *Blood* **118,** 5573–5582
28. Noushmehr, H., Weisenberger, D. J., Diefes, K., Phillips, H. S., Pujara, K., Berman, B. P., Pan, F., Pelloski, C. E., Sulman, E. P., Bhat, K. P., Verhaak, R. G., Hoadley, K. A., Hayes, D. N., Perou, C. M., Schmidt, H. K., Ding, L., Wilson, R. K., Van Den Berg, D., Shen, H., Bengtsson, H., Neuvial, P., Cope, L. M., Buckley, J., Herman, J. G., Baylin, S. B., Laird, P. W., and Aldape, K. (2010) Identification of a CpG island methylator phenotype that defines a distinct subgroup of glioma. *Cancer Cell* **17,** 510–522
29. Chowdhury, R., Yeoh, K. K., Tian, Y. M., Hillringhaus, L., Bagg, E. A., Rose, N. R., Leung, I. K., Li, X. S., Woon, E. C., Yang, M., McDonough, M. A., King, O. N., Clifton, I. J., Klose, R. J., Claridge, T. D., Ratcliffe, P. J., Schofield, C. J., and Kawamura, A. (2011) The oncometabolite 2-hydroxyglutarate inhibits histone lysine demethylases. *EMBO Rep.* **12,** 463–469
30. Figueroa, M. E., Abdel-Wahab, O., Lu, C., Ward, P. S., Patel, J., Shih, A., Li, Y., Bhagwat, N., Vasanthakumar, A., Fernandez, H. F., Tallman, M. S., Sun, Z., Wolniak, K., Peeters, J. K., Liu, W., Choe, S. E., Fantin, V. R., Paietta, E., Löwenberg, B., Licht, J. D., Godley, L. A., Delwel, R., Valk, P. J., Thompson, C. B., Levine, R. L., and Melnick, A. (2010) Leukemic IDH1 and IDH2 mutations result in a hypermethylation phenotype, disrupt TET2 function, and impair hematopoietic differentiation. *Cancer Cell* **18,** 553–567
31. Zhao, S., Lin, Y., Xu, W., Jiang, W., Zha, Z., Wang, P., Yu, W., Li, Z., Gong, L., Peng, Y., Ding, J., Lei, Q., Guan, K. L., and Xiong, Y. (2009) Glioma-derived mutations in IDH1 dominantly inhibit IDH1 catalytic activity and induce HIF-1α. *Science* **324,** 261–265
32. Sasaki, M., Knobbe, C. B., Munger, J. C., Lind, E. F., Brenner, D., Brüstle, A., Harris, I. S., Holmes, R., Wakeham, A., Haight, J., You-Ten, A., Li, W. Y., Schalm, S., Su, S. M., Virtanen, C., Reifenberger, G., Ohashi, P. S., Barber, D. L., Figueroa, M. E., Melnick, A., Zúñiga-Pflücker, J. C., and Mak, T. W. (2012) IDH1(R132H) mutation increases murine haematopoietic progenitors and alters epigenetics. *Nature* **488,** 656–659
33. Sasaki, M., Knobbe, C. B., Itsumi, M., Elia, A. J., Harris, I. S., Chio, I. I., Cairns, R. A., McCracken, S., Wakeham, A., Haight, J., Ten, A. Y., Snow, B., Ueda, T., Inoue, S., Yamamoto, K., Ko, M., Rao, A., Yen, K. E., Su, S. M., and Mak, T. W. (2012) D-2-Hydroxyglutarate produced by mutant IDH1 perturbs collagen maturation and basement membrane function. *Genes Dev.* **26,** 2038–2049
34. Turcan, S., Rohle, D., Goenka, A., Walsh, L. A., Fang, F., Yilmaz, E., Campos, C., Fabius, A. W., Lu, C., Ward, P. S., Thompson, C. B., Kaufman, A., Guryanova, O., Levine, R., Heguy, A., Viale, A., Morris, L. G., Huse, J. T., Mellinghoff, I. K., and Chan, T. A. (2012) IDH1 mutation is sufficient to establish the glioma hypermethylator phenotype. *Nature* **483,** 479–483
35. Barretina, J., Caponigro, G., Stransky, N., Venkatesan, K., Margolin, A. A., Kim, S., Wilson, C. J., Lehár, J., Kryukov, G. V., Sonkin, D., Reddy, A., Liu, M., Murray, L., Berger, M. F., Monahan, J. E., Morais, P., Meltzer, J., Korejwa, A., Jané-Valbuena, J., Mapa, F. A., Thibault, J., Bric-Furlong, E., Raman, P., Shipway, A., Engels, I. H., Cheng, J., Yu, G. K., Yu, J., Aspesi, P., Jr., de Silva, M., Jagtap, K., Jones, M. D., Wang, L., Hatton, C., Palescandolo, E., Gupta, S., Mahan, S., Sougnez, C., Onofrio, R. C., Liefeld, T., MacConaill, L., Winckler, W., Reich, M., Li, N., Mesirov, J. P., Gabriel, S. B., Getz, G., Ardlie, K., Chan, V., Myer, V. E., Weber, B. L., Porter, J., Warmuth, M., Finan, P., Harris, J. L., Meyerson, M., Golub, T. R., Morrissey, M. P., Sellers, W. R., Schlegel, R., and Garraway, L. A. (2012) The Cancer Cell Line Encyclopedia enables predictive modeling of anticancer drug sensitivity. *Nature* **483,** 603–607
36. Kohli, M., Rago, C., Lengauer, C., Kinzler, K. W., and Vogelstein, B. (2004) Facile methods for generating human somatic cell gene knockouts using recombinant adeno-associated viruses. *Nucleic Acids Res.* **32,** e3
37. Debnath, J., Muthuswamy, S. K., and Brugge, J. S. (2003) Morphogenesis and oncogenesis of MCF-10A mammary epithelial acini grown in three-dimensional basement membrane cultures. *Methods* **30,** 256–268
38. Grassian, A. R., Metallo, C. M., Coloff, J. L., Stephanopoulos, G., and Brugge, J. S. (2011) Erk regulation of pyruvate dehydrogenase flux through PDK4 modulates cell proliferation. *Genes Dev.* **25,** 1716–1733
39. Wiederschain, D., Chen, L., Johnson, B., Bettano, K., Jackson, D., Taraszka, J., Wang, Y. K., Jones, M. D., Morrissey, M., Deeds, J., Mosher, R., Fordjour, P., Lengauer, C., and Benson, J. D. (2007) Contribution of polycomb homologues Bmi-1 and Mel-18 to medulloblastoma pathogenesis. *Mol. Cell. Biol.* **27,** 4968–4979
40. Taube, J. H., Herschkowitz, J. I., Komurov, K., Zhou, A. Y., Gupta, S., Yang, J., Hartwell, K., Onder, T. T., Gupta, P. B., Evans, K. W., Hollier, B. G., Ram, P. T., Lander, E. S., Rosen, J. M., Weinberg, R. A., and Mani, S. A. (2010) Core epithelial-to-mesenchymal transition interactome gene-expression signature is associated with claudin-low and metaplastic breast cancer subtypes. *Proc. Natl. Acad. Sci. U.S.A.* **107,** 15449–15454
41. Blick, T., Hugo, H., Widodo, E., Waltham, M., Pinto, C., Mani, S. A., Weinberg, R. A., Neve, R. M., Lenburg, M. E., and Thompson, E. W. (2010) Epithelial mesenchymal transition traits in human breast cancer cell lines parallel the CD44(hi/)CD24 (lo/−) stem cell phenotype in human breast cancer. *J. Mammary Gland Biol. Neoplasia* **15,** 235–252
42. Loboda, A., Nebozhyn, M. V., Watters, J. W., Buser, C. A., Shaw, P. M., Huang, P. S., Van't Veer, L., Tollenaar, R. A., Jackson, D. B., Agrawal, D., Dai, H., and Yeatman, T. J. (2011) EMT is the dominant program in human colon cancer. *BMC Med. Genomics* **4,** 9
43. Wiederschain, D., Wee, S., Chen, L., Loo, A., Yang, G., Huang, A., Chen, Y., Caponigro, G., Yao, Y. M., Lengauer, C., Sellers, W. R., and Benson, J. D. (2009) Single-vector inducible lentiviral RNAi system for oncology target validation. *Cell Cycle* **8,** 498–504
44. Wee, S., Wiederschain, D., Maira, S. M., Loo, A., Miller, C., deBeaumont, R., Stegmeier, F., Yao, Y. M., and Lengauer, C. (2008) PTEN-deficient cancers depend on PIK3CB. *Proc. Natl. Acad. Sci. U.S.A.* **105,** 13057–13062
45. Capper, D., Zentgraf, H., Balss, J., Hartmann, C., and von Deimling, A. (2009) Monoclonal antibody specific for IDH1 R132H mutation. *Acta Neuropathol.* **118,** 599–601
46. Kalluri, R., and Weinberg, R. A. (2009) The basics of epithelial-mesenchymal transition. *J. Clin. Invest.* **119,** 1420–1428
47. Schmalhofer, O., Brabletz, S., and Brabletz, T. (2009) E-cadherin, β-catenin, and ZEB1 in malignant progression of cancer. *Cancer Metastasis Rev.* **28,** 151–166
48. Park, S. M., Gaur, A. B., Lengyel, E., and Peter, M. E. (2008) The miR-200 family determines the epithelial phenotype of cancer cells by targeting the E-cadherin repressors ZEB1 and ZEB2. *Genes Dev.* **22,** 894–907
49. Korpal, M., Lee, E. S., Hu, G., and Kang, Y. (2008) The miR-200 family inhibits epithelial-mesenchymal transition and cancer cell migration by direct targeting of E-cadherin transcriptional repressors ZEB1 and ZEB2. *J. Biol. Chem.* **283,** 14910–14914
50. Hurteau, G. J., Carlson, J. A., Spivack, S. D., and Brock, G. J. (2007) Overexpression of the microRNA hsa-miR-200c leads to reduced expression of transcription factor 8 and increased expression of E-cadherin. *Cancer Res.* **67,** 7972–7976
51. Gregory, P. A., Bert, A. G., Paterson, E. L., Barry, S. C., Tsykin, A., Farshid, G., Vadas, M. A., Khew-Goodall, Y., and Goodall, G. J. (2008) The miR-200 family and miR-205 regulate epithelial to mesenchymal transition by targeting ZEB1 and SIP1. *Nat. Cell Biol.* **10,** 593–601
52. Christoffersen, N. R., Silahtaroglu, A., Orom, U. A., Kauppinen, S., and Lund, A. H. (2007) miR-200b mediates post-transcriptional repression of ZFHX1B. *RNA* **13,** 1172–1178
53. Burk, U., Schubert, J., Wellner, U., Schmalhofer, O., Vincan, E., Spaderna, S., and Brabletz, T. (2008) A reciprocal repression between ZEB1 and members of the miR-200 family promotes EMT and invasion in cancer cells. *EMBO Rep.* **9,** 582–589
54. Brabletz, S., and Brabletz, T. (2010) The ZEB/miR-200 feedback loop–a motor of cellular plasticity in development and cancer? *EMBO Rep.* **11,** 670–677
55. Edwards, S. L., Brough, R., Lord, C. J., Natrajan, R., Vatcheva, R., Levine, D. A., Boyd, J., Reis-Filho, J. S., and Ashworth, A. (2008) Resistance to therapy caused by intragenic deletion in BRCA2. *Nature* **451,** 1111–1115
56. Popovici-Muller, J., Saunders, J. O., Salituro, F. G., Travins, J. M., Yan, S., Zhao, F., Gross, S., Dang, L., Yen, K. E., Yang, H., Straley, K. S., Jin, S., Kunii, K., Fantin, V. R., Zhang, S., Pan, Q., Shi, D., Biller, S. A., and Su, S. M. (2012) Discovery of the first potent inhibitors of mutant IDH1 that lower tumor 2-HG *in vivo*. *ACS Med. Chem. Lett.* **3,** 850–855
57. Duncan, C. G., Barwick, B. G., Jin, G., Rago, C., Kapoor-Vazirani, P., Powell, D. R., Chi, J. T., Bigner, D. D., Vertino, P. M., and Yan, H. (2012) A

heterozygous IDH1R132H/WT mutation induces genome-wide alterations in DNA methylation. *Genome Res.*, in press
58. Hathaway, N. A., Bell, O., Hodges, C., Miller, E. L., Neel, D. S., and Crabtree, G. R. (2012) Dynamics and memory of heterochromatin in living cells. *Cell* **149,** 1447–1460
59. Singh, A., and Settleman, J. (2010) EMT, cancer stem cells and drug resistance. An emerging axis of evil in the war on cancer. *Oncogene* **29,** 4741–4751
60. Scheel, C., and Weinberg, R. A. (2012) Cancer stem cells and epithelial-mesenchymal transition. Concepts and molecular links. *Semin. Cancer Biol.* **22,** 396–403
61. Oishi, N., Kumar, M. R., Roessler, S., Ji, J., Forgues, M., Budhu, A., Zhao, X., Andersen, J. B., Ye, Q. H., Jia, H. L., Qin, L. X., Yamashita, T., Goo Woo, H., Jun Kim, Y., Kaneko, S., Tang, Z. Y., Thorgeirsson, S. S., and Wei Wang, X. (2012) Transcriptomic profiling reveals hepatic stem-like gene signatures and interplay of miR-200c and epithelial-mesenchymal transition in intrahepatic cholangiocarcinoma. *Hepatology* 2012 Jun 18. doi: 10.1002/hep.25890
62. Sellner, L., Capper, D., Meyer, J., Langhans, C. D., Hartog, C. M., Pfeifer, H., Serve, H., Ho, A. D., Okun, J. G., Krämer, A., and Von Deimling, A. (2010) Increased levels of 2-hydroxyglutarate in AML patients with IDH1-R132H and IDH2-R140Q mutations. *Eur. J. Haematol.* **85,** 457–459
63. Chou, W. C., Lei, W. C., Ko, B. S., Hou, H. A., Chen, C. Y., Tang, J. L., Yao, M., Tsay, W., Wu, S. J., Huang, S. Y., Hsu, S. C., Chen, Y. C., Chang, Y. C., Kuo, K. T., Lee, F. Y., Liu, M. C., Liu, C. W., Tseng, M. H., Huang, C. F., and Tien, H. F. (2011) The prognostic impact and stability of isocitrate dehydrogenase 2 mutation in adult patients with acute myeloid leukemia. *Leukemia* **25,** 246–253
64. Herranz, H., and Cohen, S. M. (2010) MicroRNAs and gene regulatory networks. Managing the impact of noise in biological systems. *Genes Dev.* **24,** 1339–1344
65. Krol, J., Loedige, I., and Filipowicz, W. (2010) The widespread regulation of microRNA biogenesis, function and decay. *Nat. Rev. Genet.* **11,** 597–610
66. Yan, Z., Shah, P. K., Amin, S. B., Samur, M. K., Huang, N., Wang, X., Misra, V., Ji, H., Gabuzda, D., and Li, C. (2012) Integrative analysis of gene and miRNA expression profiles with transcription factor-miRNA feed-forward loops identifies regulators in human cancers. *Nucleic Acids Res.* **40,** e135